Conformation-selective resonant photoelectron imaging from dipole-bound states of cold 3-hydroxyphenoxide

Guo-Zhu Zhu, Dao-Ling Huang, and Lai-Sheng Wang

Citation: The Journal of Chemical Physics **147**, 013910 (2017); doi: 10.1063/1.4979331
View online: http://dx.doi.org/10.1063/1.4979331
View Table of Contents: http://aip.scitation.org/toc/jcp/147/1
Published by the American Institute of Physics

Conformation-selective resonant photoelectron imaging from dipole-bound states of cold 3-hydroxyphenoxide

Guo-Zhu Zhu,[a] Dao-Ling Huang,[a] and Lai-Sheng Wang[b]
Department of Chemistry, Brown University, Providence, Rhode Island 02912, USA

(Received 30 January 2017; accepted 15 March 2017; published online 3 April 2017)

We report a photoelectron imaging and photodetachment study of cryogenically cooled 3-hydroxyphenoxide (3HOP) anions, *m*-$HO(C_6H_4)O^-$. In a previous preliminary study, two conformations of the cold 3HOP anions with different dipole bound states were observed [D. L. Huang *et al.*, J. Phys. Chem. Lett. **6**, 2153 (2015)]. Five near-threshold vibrational resonances were revealed in the photodetachment spectrum from the dipole-bound excited states of the two conformations. Here, we report a more extensive investigation of the two conformers with observation of thirty above-threshold vibrational resonances in a wide spectral range between 18 850 and 19 920 cm^{-1} (~1000 cm^{-1} above the detachment thresholds). By tuning the detachment laser to the vibrational resonances in the photodetachment spectrum, high-resolution conformation-selective resonant photoelectron images are obtained. Using information of the autodetachment channels and theoretical vibrational frequencies, we are able to assign the resonant peaks in the photodetachment spectrum: seventeen are assigned to vibrational levels of *anti*-3HOP, eight to *syn*-3HOP, and five to overlapping vibrational levels of both conformers. From the photodetachment spectrum and the conformation-selective resonant photoelectron spectra, we have obtained fourteen fundamental vibrational frequencies for the neutral *syn*- and *anti*-*m*-$HO(C_6H_4)O^{\cdot}$ radicals. The possibility to produce conformation-selected neutral beams using resonant photodetachment via dipole-bound excited states of anions is discussed. *Published by AIP Publishing.* [http://dx.doi.org/10.1063/1.4979331]

I. INTRODUCTION

The semiquinone radicals, $HO(C_6H_4)O^{\cdot}$, are important electron transfer intermediates in biological processes such as photosynthesis and respiration.[1–3] Different from the *o*- and *p*-$HO(C_6H_4)O^{\cdot}$ isomers, the 3-hydroxyphenoxy radical [*m*-$HO(C_6H_4)O^{\cdot}$] is particularly interesting, because it can exist as two close-lying conformers, *anti*- and *syn*-*m*-$HO(C_6H_4)O^{\cdot}$. The two conformations differ by the orientations of the hydrogen atom on the hydroxyl group,[4,5] as shown in Fig. 1, along with their respective precursor anions. The two conformers of the 3-hydroxyphenoxy radical have different dipole moments and can support dipole-bound states (DBS) with different binding energies (BEs).[6–9] In a previous preliminary study,[10] we observed the two conformations in high-resolution photoelectron imaging (PEI) of cryogenically cooled 3-hydroxyphenoxide (3HOP) anions, *m*-$HO(C_6H_4)O^-$. The electron binding energies of the two 3HOP conformations or the electron affinities of the *anti*- and *syn*-*m*-$HO(C_6H_4)O^{\cdot}$ radicals were found to differ by 67 cm^{-1} with the *anti*-conformer being slightly higher. More interestingly, the two conformers of the anion were found to possess excited DBS with different binding energies relative to the respective detachment thresholds, 490 cm^{-1} and 104 cm^{-1} for the *anti*- and *syn*-3HOP, respectively. Five near-threshold vibrational resonances were observed and conformation-selective PEI was realized via the vibrational levels of the DBS. In the current article, we report a more comprehensive investigation of the 3HOP anion in a wider spectral range, yielding extensive vibrational information for the two conformers of the *m*-$HO(C_6H_4)O^{\cdot}$ radicals.

Molecular conformations are important in chemistry and biochemistry.[11–14] Several experimental techniques have been used to characterize conformational structures and dynamics, such as microwave spectroscopy,[15] infrared (IR) spectroscopy,[13–16] and conformer-specific photodissociation dynamics and spectroscopy.[17–19] Conformers of neutral molecules with sufficiently different dipole moments can be selected using the Stark effects to probe conformation-dependent chemical reactivity.[20,21] High-resolution resonant photoelectron imaging via dipole-bound excited states of cold anions yields conformation-selective photoelectron spectra and can be considered as a new method to obtain conformation-selective spectroscopic information for dipolar molecular radicals.[10]

This method is based on mode-specific vibrational autodetachment from vibrational levels of DBS, first observed in cryogenically cooled phenoxide anions.[22,23] Due to the $\Delta v = -1$ propensity rule,[24,25] highly non-Franck-Condon resonant PE spectra were obtained to yield much more vibrational information, particularly for low-frequency and Franck-Condon-inactive vibrational modes.[26–32] Beyond the preliminary observation of five vibrational resonances due to the excited DBS of *anti*- and *syn*-3HOP,[10] here we report photodetachment spectroscopy with photon energies up to

[a] G.-Z. Zhu and D.-L. Huang contributed equally to this work.
[b] Email: Lai-Sheng_Wang@brown.edu

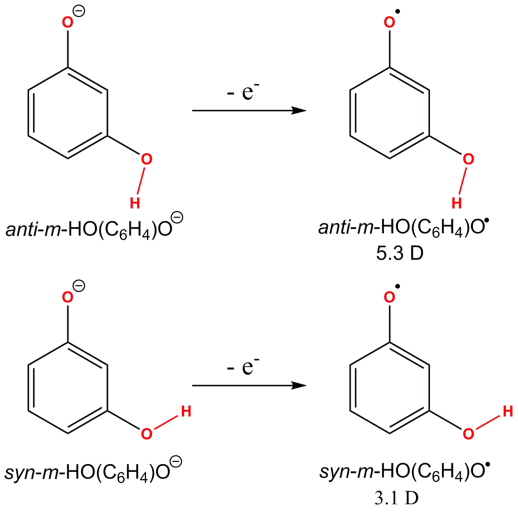

FIG. 1. The structures of the *anti*- and *syn*-conformation of *m*-$HO(C_6H_4)O^-$ and the corresponding neutral *m*-$HO(C_6H_4)O^{\cdot}$ radicals along with their dipole moments.

~1000 cm^{-1} above the detachment thresholds. A total of thirty vibrational resonances are observed, seventeen from the *anti*-3HOP conformer, eight from the *syn*-3HOP conformer, and five from overlapping vibrational levels of the DBS of both conformers. Conformation-selective resonant PE images have been obtained by tuning the detachment laser to the vibrational resonances. The photodetachment spectrum is assigned using the resonant PE spectra in conjunction with computed vibrational frequencies. Based on the photodetachment spectrum and resonant PE images, we are able to obtain fourteen fundamental vibrational frequencies for each of the *m*-$HO(C_6H_4)O^{\cdot}$ conformations.

II. EXPERIMENTAL METHODS

The experiment was done using our third-generation electrospray-photoelectron spectroscopy apparatus,[23] equipped with a cryogenically cooled Paul trap[33] and a high-resolution PE imaging system.[34] The 3HOP anions were produced by deprotonation of *m*-$HO(C_6H_4)OH$ via electrospray of a 1 mM solution in a mixed solvent of CH_3OH/H_2O (9/1 in volume) at pH ~ 10. Anions generated in the electrospray ionization source were guided into a cryogenically cooled Paul trap operated at 4.5 K. After being accumulated for 0.1 s and thermally cooled via collisions with 1 mTorr He/H_2 (4/1 in volume) background gas,[23,33] the anions were pulsed out at a 10 Hz repetition rate into the extraction zone of a time-of-flight mass spectrometer. The 3HOP anions were selected by a mass gate and photodetached in the interaction zone of the imaging lens by a dye laser. Photoelectrons were projected onto a pair of 75-mm diameter micro-channel plates coupled to a phosphor screen and captured by a charge-coupled device camera. The PE images were inverse-Abel transformed and reconstructed using the pBasex and BASEX programs.[35,36] The PE spectra were calibrated with the known spectra of Au^- at different photon energies. The kinetic energy (KE) resolution achieved was 3.8 cm^{-1} for electrons with 55 cm^{-1} KE and about 1.5% (ΔKE/KE) for KE above 1 eV in the current experiment.

III. RESULTS

A. Non-resonant photoelectron images and spectra

Fig. 2 shows the non-resonant PE images and spectra of *m*-$HO(C_6H_4)O^-$ at two photon energies. At 517.45 nm, three peaks, labeled as $^S0_0^0$, $^A0_0^0$, and A, are resolved. The superscripts "S" and "A" in the labels and throughout the text are used to designate the *syn* and *anti* conformations. As discussed in Ref. 10, peaks $^S0_0^0$ and $^A0_0^0$ at binding energies of 18 850 cm^{-1} and 18 917 cm^{-1} represent the vibrational origins of the *syn*- and *anti*-*m*-$HO(C_6H_4)O^{\cdot}$ radical conformations or their electron affinities, respectively. It should be noted that vibrational hot bands are completely eliminated due to the effective vibrational cooling in the cryogenic ion trap.[22,23,37–39] Peak A corresponds to the fundamental vibrational excitation of mode $^S\nu_{23}$ of *syn*-*m*-$HO(C_6H_4)O^{\cdot}$. The relative high intensity of peak A is due to the near-threshold enhancement.[10] At 501.01 nm, the normal Franck-Condon profiles are displayed for vibrational peaks far from threshold (the two near-threshold peaks L and M are enhanced). Peaks A–M correspond to transitions from the ground states of the *anti*- and *syn*-*m*-3HOP anions to different excited vibrational levels of the *anti*- and *syn*-*m*-$HO(C_6H_4)O^{\cdot}$ neutral radicals. The electron binding energies of all the observed vibrational peaks, their shifts from the respective vibrational origins, and assignments are summarized in Table I, where the more accurate values are from the resonant PE spectra to be presented below.

B. Photodetachment spectroscopy

Fig. 3 shows the photodetachment spectrum of 3HOP with photon energy ~1000 cm^{-1} above the detachment thresholds, labeled as ^{S}EA and ^{A}EA for the *syn*- and *anti*-3HOP conformers, respectively. This spectrum was obtained by monitoring the total electron yield while scanning the dye laser wavelength near and above the detachment thresholds of 3HOP.[37] The overall baseline above thresholds represents the cross section of direct non-resonant photodetachment of 3HOP. Thirty above-threshold resonances are observed and labeled as

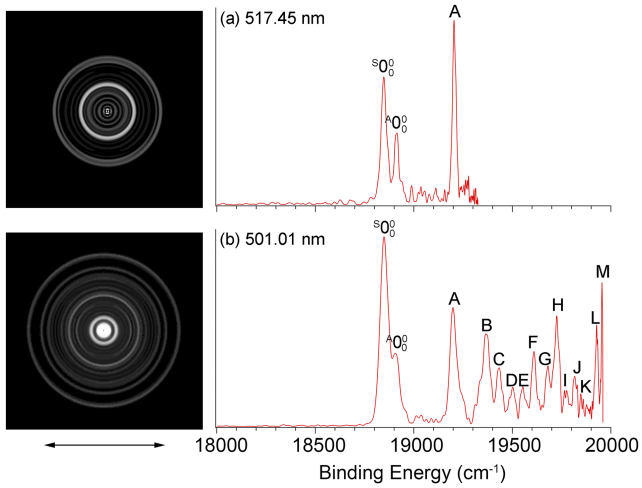

FIG. 2. Non-resonant photoelectron images and spectra of *m*-$HO(C_6H_4)O^-$ at (a) 517.45 nm and (b) 501.01 nm. The double arrow below the images indicates the direction of the laser polarization.

TABLE I. The observed vibrational peaks and their binding energies (BEs) from the photoelectron spectra of *m*-$HO(C_6H_4)O^-$. The energy shifts from the vibrational origins of *anti*- and *syn*-*m*-$HO(C_6H_4)O^{\cdot}$ are given. Peaks A–M correspond to those in the non-resonant photoelectron spectra in Fig. 2, while peaks a–h are from the resonant photoelectron spectra in Figs. 5 and 6. The binding energies of peaks $^{S}0_0^{0}$, $^{A}0_0^{0}$, and A–J are measured more accurately from the resonant photoelectron spectra in Figs. 4–6.

Peaks	BE (cm^{-1})[a]	Shift to $^{S}0_0^{0}$ (cm^{-1})	Shift to $^{A}0_0^{0}$ (cm^{-1})	Assignment[b]
$^{S}0_0^{0}$	18 850(5)	0		Neutral ground state (S)
$^{A}0_0^{0}$	18 917(5)		0	Neutral ground state (A)
A	19 207(5)	357		$^{S}23^{1}$
B	19 365(5)	515		$^{S}21^{1}$
C	19 435(5)		518	$^{A}21^{1}$
D	19 498(5)		581	$^{A}29^{1}$
E	19 560(5)	710	643	$^{A}28^{1}/^{S}23^{2}$
F	19 613(5)	763		$^{S}27^{1}$
G	19 680(5)		763	$^{A}27^{1}$
H	19 725(5)	875		$^{S}25^{1}/^{S}21^{1}23^{1}$
I	19 775(5)		858	$^{A}25^{1}$
J	19 828(5)		911	$^{A}18^{1}$
K	19 849(10)	999		$^{S}17^{1}$
L	19 929(10)	1079		$^{S}23^{3}$
M	19 955(10)		1038	$^{A}21^{2}$
a	19 034(5)	184		$^{S}33^{1}$
b	19 092(5)		175	$^{A}33^{1}$
c	19 120(5)		203	$^{A}32^{1}$
d	19 268(5)	418		$^{S}30^{1}$
e	19 336(5)	486		$^{S}22^{1}$
f	19 402(5)		485	$^{A}22^{1}$
g	19 880(5)		963	$^{A}24^{1}$
h	19 750(5)		833	$^{A}26^{1}$

[a]Numbers in parentheses in BE indicate the experimental uncertainties.
[b]The A and S labels refer to final states for the anti- and syn-conformers, respectively.

$^{A}1$–$^{A}17$ (blue), $^{S}1$–$^{S}8$ (red), and $^{AS}1$–$^{AS}5$ (pink). These peaks indicate autodetachment from vibrational levels of the excited DBS of *anti*-3HOP, *syn*-3HOP, and overlapping levels of both conformers, respectively. The first five peaks ($^{A}1$–$^{A}4$ and $^{S}1$)

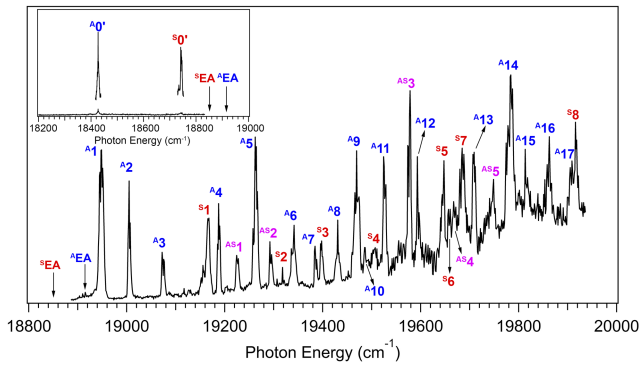

FIG. 3. The photodetachment spectrum of *m*-$HO(C_6H_4)O^-$ by measuring the total electron yield as a function of photon energy near and above the detachment thresholds. The two arrows (^{A}EA and ^{S}EA) indicate the detachment thresholds for *anti*- and *syn*-*m*-$HO(C_6H_4)O^-$, respectively. The peaks labeled as $^{A}1$–$^{A}17$ (blue) are due to autodetachment from DBS vibrational levels of *anti*-*m*-$HO(C_6H_4)O^-$, while peaks $^{S}1$–$^{S}8$ (red) are from *syn*-*m*-$HO(C_6H_4)O^-$ and peaks $^{AS}1$–$^{AS}5$ (pink) are from both anion conformers. The inset shows the photodetachment spectrum below the detachment threshold and the two peaks, labeled as $^{A}0'$ and $^{S}0'$, represent the ground DBS of *anti*- and *syn*-*m*-$HO(C_6H_4)O^-$, respectively.[10]

were reported in the previous preliminary study[10] as well as the below-threshold vibrational origins of the DBS of the two conformers shown in the inset ($^{A}0'$ and $^{S}0'$. Note a $'$ sign is used to designate vibrational levels of the DBS). The two below-threshold origin peaks were very weak, because they were due to two-photon detachment. The $^{A}0'$ and $^{S}0'$ peaks defined the DBS binding energies of 490 and 104 cm^{-1} for the *anti*- and *syn*-3HOP conformers, relative to their respective detachment thresholds (^{A}EA and ^{S}EA).[10] The larger DBS binding energy of the *anti*-conformer is consistent with the larger dipole moment of the neutral radical (Fig. 1). The photon energies, shifts from the respective ground DBS vibrational levels, and assignments of the observed resonances are given in Table II. The assignments of all the vibrational peaks are based on the autodetachment in the resonant PE spectra shown in Figs. 4–6 and the calculated vibrational frequencies given in Table III.

TABLE II. The observed peaks, photon energies (hv), shifts from the ground DBS of *anti*- and *syn*-*m*-$HO(C_6H_4)O^-$, and assignments for the photodetachment spectrum in Fig. 3.

Peak[a]	hv (cm^{-1})[b]	Shift (cm^{-1})	Assignment
$^{A}0'$	18 427(5)		Ground DBS of *anti*
$^{A}1$	18 949(5)	(A)522	$^{A}21'^{1}$
$^{A}2$	19 006(5)	(A)579	$^{A}29'^{1}$
$^{A}3$	19 073(5)	(A)646	$^{A}28'^{1}$
$^{A}4$	19 188(5)	(A)761	$^{A}27'^{1}$
$^{A}5$	19 259(5)	(A)832	$^{A}26'^{1}$
$^{A}6$	19 342(5)	(A)915	$^{A}18'^{1}$
$^{A}7$	19 386(5)	(A)959	$^{A}24'^{1}$
$^{A}8$	19 431(5)	(A)1004	$^{A}21'^{1}22'^{1}$
$^{A}9$	19 470(5)	(A)1043	$^{A}21'^{2}$
$^{A}10$	19 486(5)	(A)1059	$^{A}22'^{1}29'^{1}$
$^{A}11$	19 525(5)	(A)1098	$^{A}21'^{1}29'^{1}$
$^{A}12$	19 594(5)	(A)1167	$^{A}14'^{1}/^{A}21'^{1}28'^{1}$
$^{A}13$	19 708(5)	(A)1281	$^{A}21'^{1}27'^{1}$
$^{A}14$	19 784(5)	(A)1357	$^{A}11'^{1}/^{A}21'^{1}26'^{1}$
$^{A}15$	19 814(5)	(A)1387	$^{A}21'^{1}25'^{1}$
$^{A}16$	19 862(5)	(A)1435	$^{A}18'^{1}21'^{1}$
$^{A}17$	19 908(5)	(A)1481	$^{A}21'^{1}24'^{1}$
$^{S}0'$	18 746(5)		Ground DBS of *syn*
$^{S}1$	19 168(5)	(S)422	$^{S}30'^{1}$
$^{S}2$	19 318(5)	(S)572	$^{S}29'^{1}/^{S}31'^{1}33'^{1}$
$^{S}3$	19 396(5)	(S)650	$^{S}28'^{1}$
$^{S}4$	19 508(5)	(S)762	$^{S}23'^{1}30'^{1}$
$^{S}5$	19 648(5)	(S)902	$^{S}22'^{1}30'^{1}$
$^{S}6$	19 658(5)	(S)912	$^{S}23'^{1}31'^{1}33'^{1}$
$^{S}7$	19 679(5)	(S)933	$^{S}18'^{1}/^{S}21'^{1}30'^{1}/^{S}27'^{1}33'^{1}$
$^{S}8$	19 917(5)	(S)1171	$^{S}21'^{1}28'^{1}/^{S}27'^{1}30'^{1}$
Overlapping levels of *anti*- and *syn*-conformers[c]			
$^{AS}1$	19 224(5)	(A)797/(S)478	$^{A}30'^{1}32'^{1}33'^{1}/^{S}22'^{1}$
$^{AS}2$	19 293(5)	(A)866/(S)547	$^{A}25'^{1}/^{A}21'^{1}33'^{2}/^{S}23'^{1}33'^{1}$
$^{AS}3$	19 578(5)	(A)1151/(S)832	$^{A}29'^{2}/^{S}26'^{1}$
$^{AS}4$	19 667(5)	(A)1240/(S)921	$^{A}22'^{1}27'^{1}/^{S}21'^{1}32'^{2}$
$^{AS}5$	19 746(5)	(A)1319/(S)1000	$^{S}17'^{1}/^{S}29'^{1}30'^{1}/^{A}27'^{1}29'^{1}$

[a]The superscripts in the peak labels indicate the conformers: A for *anti*, S for *syn*, and AS for overlapping levels of the *anti*- and *syn*-conformers.
[b]Numbers in parentheses indicate the experimental uncertainties.
[c]Shifts for the *anti*-conformer are referenced to $^{A}0'$ and those for the *syn*-conformer are referenced to $^{S}0'$.

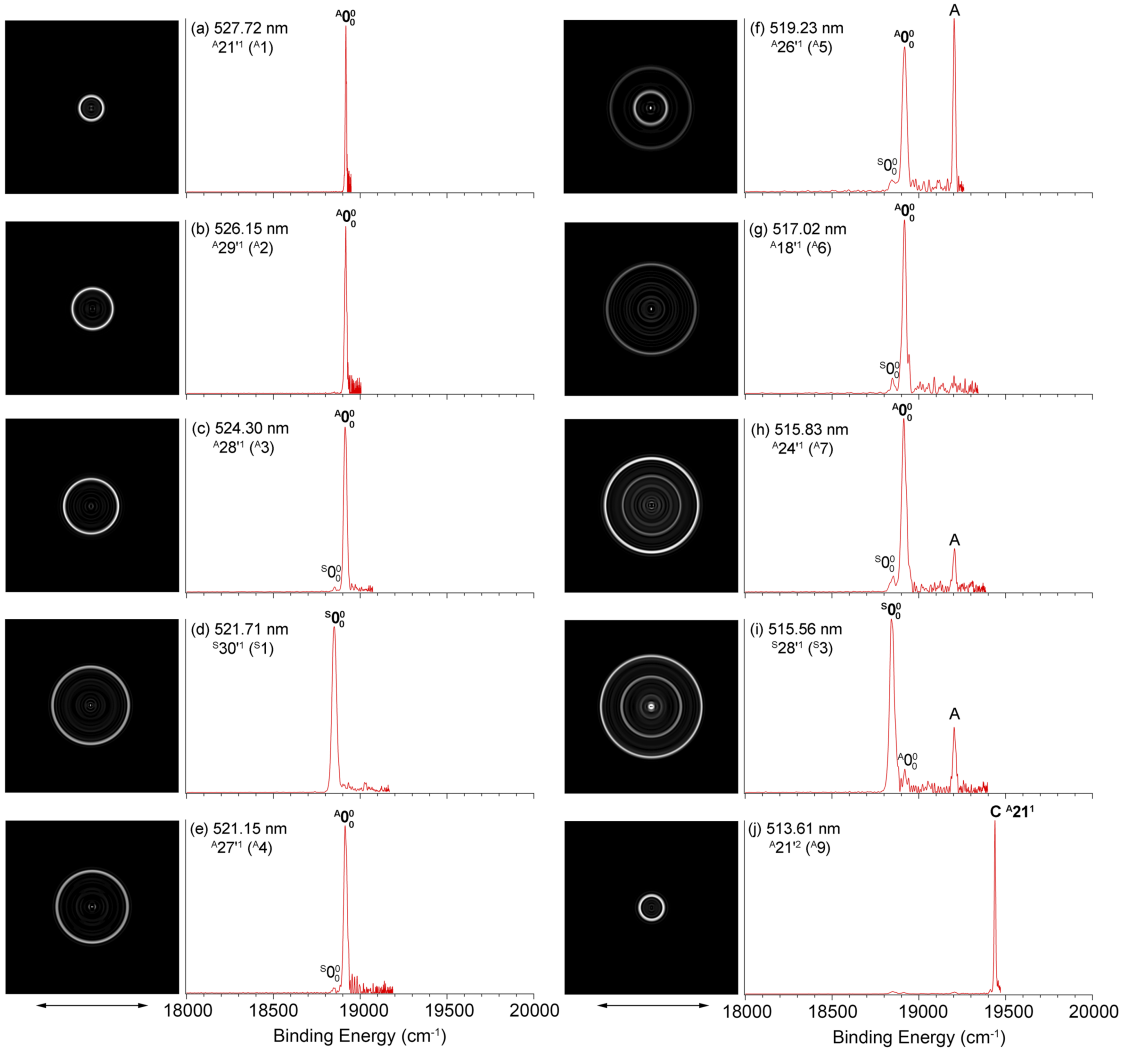

FIG. 4. Resonant photoelectron images and spectra of *m*-HO(C_6H_4)O^- at ten different detachment wavelengths, corresponding to autodetachment involving single vibrational modes. The peak number (in parentheses) corresponds to that in Fig. 3 and the assigned DBS vibrational levels are given. The labels in bold face indicate the autodetachment-enhanced final neutral vibrational levels. And the double arrow below the images represents the direction of the laser polarization.

C. Resonant photoelectron images and spectra

By tuning the detachment laser to the above-threshold resonances in Fig. 3, we obtained thirty high-resolution resonantly enhanced PE images and spectra, as shown in Figs. 4–6. The detachment laser wavelength, the DBS vibrational level, and the corresponding peak label (in parentheses) used in the photodetachment spectrum of Fig. 3 are given in each resonant PE spectrum in Figs. 4–6. The resonant excitations involve different vibrational levels of the DBS of the two conformers of 3HOP, followed by autodetachment. The ten spectra in Fig. 4 contain autodetachment involving a single vibrational mode of the DBS, where the five spectra on the left, reported previously,[10] are shown here for completeness and for comparison. The ten spectra in Fig. 5 represent excitations to combinational vibrational levels of the DBS, whereas the ten spectra in Fig. 6 correspond to excitations to overlapping vibrational levels of DBS of the two conformers. These resonant PE spectra involve two detachment channels:[22] (1) non-resonant direct photodetachment represented by the baseline in Fig. 3 and (2) resonant autodetachment via the DBS represented by the resonances in Fig. 3. Due to mode-selectivity and the $\Delta v = -1$ propensity rule in the autodetachment process, highly non-Franck-Condon spectra are obtained, with certain vibrational levels significantly enhanced.[26–32] The enhanced vibrational levels in each spectrum are labeled in bold face. In addition, several vibrational peaks not observed in the non-resonant PE spectra in Fig. 2 appear in the resonant PE spectra in Figs. 5 and 6. They are labeled as a–h; their binding energies and assignments are also given in Table I.

IV. DISCUSSION

A. Assignments of the non-resonant photoelectron spectra

To assist the assignment of the vibrational peaks in the PE spectra, we calculated the vibrational frequencies of *anti*- and *syn*-*m*-HO(C_6H_4)O$^\cdot$ at the B3LYP/6-311++G(d,p) level, as shown in Table III. The vibrational modes and frequencies of the two conformers are very similar as expected, except the ν_{31} mode, which corresponds to the out-of-plane rocking mode of the OH group (Fig. 7). Since both the anions and the neutral radicals of the two conformers are planar with C_s symmetry, only in-plane modes (A′) or even quanta of out-of-plane modes

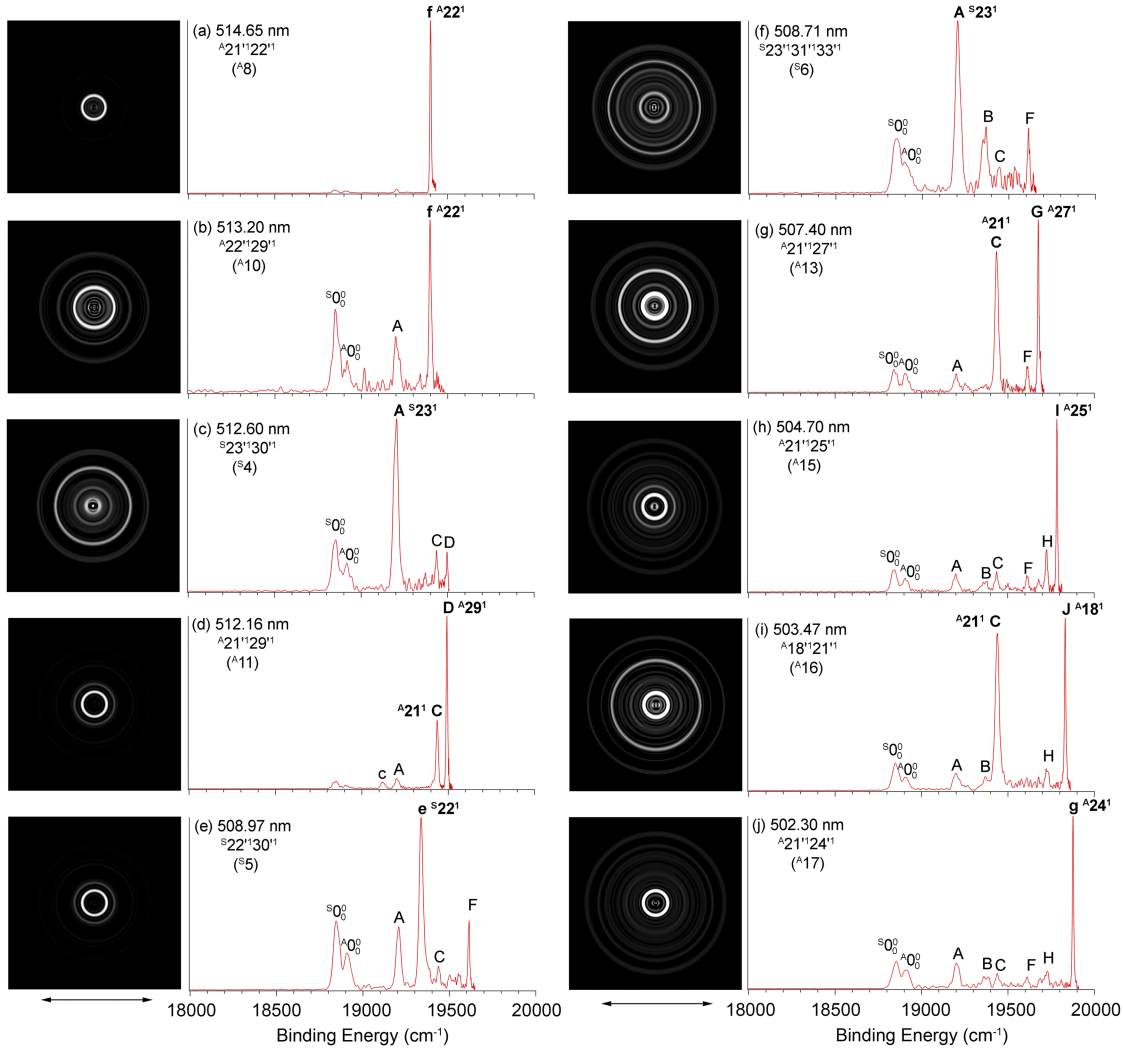

FIG. 5. Resonant photoelectron images and spectra of *m*-HO(C_6H_4)O^- at ten different detachment wavelengths, representing autodetachment involving combinational DBS vibrational levels. The peak number (in parentheses) corresponds to that in Fig. 3 and the assigned DBS vibrational levels are given. The labels in bold face indicate the autodetachment-enhanced final neutral vibrational levels. And the double arrows below the images represent the direction of the laser polarization.

(A″) are allowed in principle in the PE spectra. The energy shifts of peaks A–M relative to the respective vibrational origins of the two conformers and their assignments are given in Table I. These peaks are due to vibrational excitations of either isomer or overlapping levels of both isomers. The assignments are accomplished by a careful comparison of the experimental shifts with the theoretical frequencies. For example, peak A has a shift of 357 cm^{-1} relative to $^{S}0_0^0$ and 290 cm^{-1} relative to $^{A}0_0^0$. The 290 cm^{-1} shift does not agree with any frequencies of the vibrational modes of *anti-m*-HO(C_6H_4)O·, while the 357 cm^{-1} shift matches well the computed frequency for the in-plane $^{S}\nu_{23}$ (A′) mode (346 cm^{-1} in Table III) of *syn-m*-HO(C_6H_4)O·. Thus, peak A is assigned to the in-plane scissoring vibrational mode $^{S}\nu_{23}$ of *syn-m*-HO(C_6H_4)O·. The energy shifts of peak B from $^{S}0_0^0$ and $^{A}0_0^0$ are 515 cm^{-1} and 448 cm^{-1}, respectively. However, the 448 cm^{-1} shift does not match any calculated frequency for *anti-m*-HO(C_6H_4)O·, while the 515 cm^{-1} shift can be readily assigned to the in-plane stretching mode $^{S}\nu_{21}$ (A′) (with a computed frequency of 509 cm^{-1} in Table III) of *syn-m*-HO(C_6H_4)O·, which is also confirmed by the autodetachment enhancement in the resonant PE spectra to be discussed below. Peak C, shifted from $^{A}0_0^0$ by 518 cm^{-1}, is assigned to the in-plane stretching mode $^{A}\nu_{21}$ (A′) (computed frequency of 511 cm^{-1} in Table III) of *anti-m*-HO(C_6H_4)O·. At higher binding energies, overlapping of vibrational levels from both conformers becomes possible, which makes the assignments difficult in some cases. Based on the autodetachment enhancement in the resonant PE spectra in Figs. 4–6, peaks D to J are assigned to $^{A}29^1$ (A″), $^{A}28^1$ (A″), $^{S}27^1$ (A″), $^{A}27^1$ (A″), $^{S}25^1$ (A″), $^{A}25^1$ (A″), and $^{A}18^1$ (A′), respectively. Interestingly, except for the in-plane mode $^{A}\nu_{18}$ (A′), the other six modes are all out-of-plane modes (A″), suggesting that the radical conformers may not be truly planar. In addition, peaks E and H can also be assigned to $^{S}23^2$ (A′) and $^{S}21^123^1$, respectively, indicating overlapping levels. Peaks K to M are assigned to $^{S}17^1$ (A′), $^{S}23^3$ (A′), and $^{A}21^2$ (A′), respectively.

B. The photodetachment spectrum

The dipole moments of *anti-* and *syn-m*-HO(C_6H_4)O· were calculated to be 5.3 D and 3.1 D, respectively

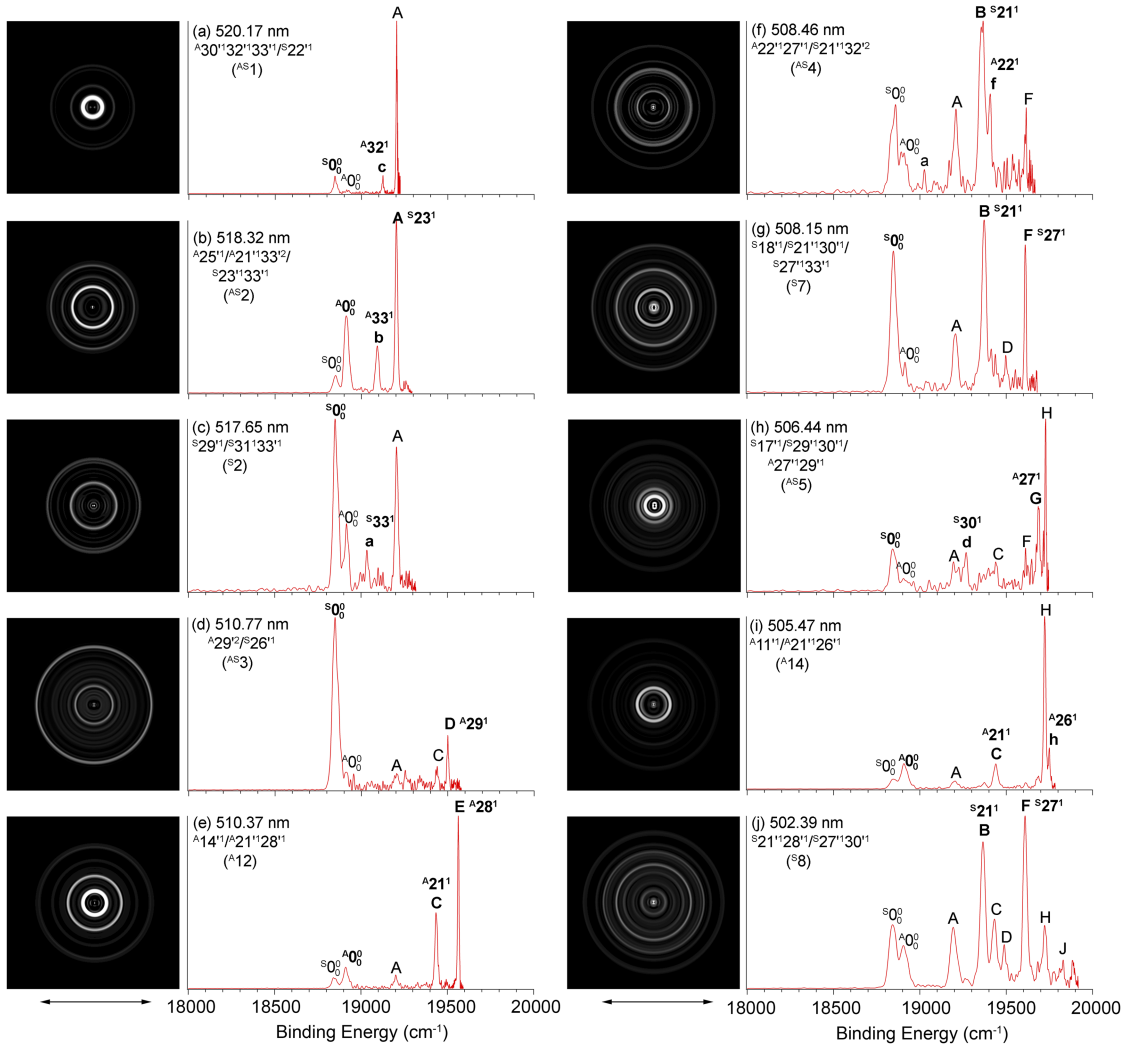

FIG. 6. Resonant photoelectron images and spectra of *m*-HO(C_6H_4)O$^-$ at ten different detachment wavelengths, representing autodetachment involving overlapping DBS vibrational levels. The peak number (in parentheses) corresponds to that in Fig. 3 and the assigned DBS vibrational levels are given. The labels in bold face indicate the autodetachment-enhanced final neutral vibrational levels. And the double arrows below the images represent the direction of the laser polarization.

(Fig. 1),[10] which are larger than the 2.5 D practical critical dipole moment to support DBS.[6] As reported in the previous preliminary study,[10] the binding energies of the DBS are 490 cm^{-1} and 104 cm^{-1} for the *anti*- and *syn*-3HOP conformers relative to their respective detachment thresholds, as shown by the below-threshold detachment peaks $^{A}0'$ and $^{S}0'$ in the inset of Fig. 3. The thirty above-threshold peaks in Fig. 3 represent optical transitions to the excited vibrational levels of the DBS of *anti*- and *syn*-3HOP, followed by autodetachment.[37] The seventeen peaks, labeled as $^{A}1$–$^{A}17$ (blue), are from vibrational levels of the DBS of the *anti*-3HOP conformer; the eight peaks, $^{S}1$–$^{S}8$ (red), are from vibrational levels of *syn*-3HOP; and the five peaks, $^{AS}1$–$^{AS}5$ (pink), are from overlapping vibrational levels of the DBS of both conformers. These assignments are done on the basis of the resonant PE spectra to be discussed below and by comparing the measured vibrational frequencies with those computed for the *anti*- and *syn*-conformers of the neutral radicals (Table III). The first five detachment peaks ($^{A}1$–$^{A}4$ and $^{S}1$) were reported in the previous preliminary study.[10] All the assignments given in Table II for these five peaks are the same, except the $^{A}1$ peak, which is reassigned to the $^{A}\nu_{21}'$ mode, instead of the $^{A}\nu_{20}'$ mode assigned previously. This reassignment is done by considering the same mode in the more extensive resonant PE spectra to be discussed below. As shown previously,[27–32] the vibrational frequencies in the DBS of anions are the same as the corresponding neutral radicals within our experimental uncertainty, because the weakly bound excess electron in the DBS has negligible influence on the structures of the neutral cores. Since the peak width in Fig. 3 is mainly limited by rotational broadening,[37] the measured frequencies in the photodetachment spectrum are in general more accurate than those obtained from the PE spectra. The near-threshold PES features have comparable accuracy as in the photodetachment spectrum. The vibrational labels for the DBS are indicated by $'$ in Table II. Most of the vibrational peaks observed in the PE spectra (Fig. 2 and Table I) are also observed in the photodetachment spectrum (Fig. 3 and Table II) with the same frequencies within the experimental accuracy.

It is interesting to note that the vibrational levels observed for the two conformers in the PE spectra in Fig. 2, as well as the photodetachment spectrum in Fig. 3, are not exactly

TABLE III. Experimental vibrational frequencies (in cm^{-1}) of *anti*- and *syn*-*m*-$HO(C_6H_4)O^{\cdot}$, in comparison to theoretical harmonic frequencies calculated at the B3LYP/6-311++G(d, p) level.

	anti-*m*-$HO(C_6H_4)O^{\cdot}$			*syn*-*m*-$HO(C_6H_4)O^{\cdot}$		
	Theo.	Expt.	Peak(s)[a]	Theo.	Expt.	Peak(s)[a]
ν_1 (A′)	3836			3827		
ν_2 (A′)	3209			3205		
ν_3 (A′)	3205			3199		
ν_4 (A′)	3180			3176		
ν_5 (A′)	3157			3175		
ν_6 (A′)	1601			1594		
ν_7 (A′)	1552			1552		
ν_8 (A′)	1474			1490		
ν_9 (A′)	1435			1444		
ν_{10} (A′)	1381			1399		
ν_{11} (A′)	1336	1357	$^{A}14$	1337		
ν_{12} (A′)	1284			1287		
ν_{13} (A′)	1227			1226		
ν_{14} (A′)	1172	1167	$^{A}12$	1179		
ν_{15} (A′)	1159			1154		
ν_{16} (A′)	1095			1091		
ν_{17} (A′)	992			989	1000/999	$^{AS}5$/K
ν_{18} (A′)	929	915/911	$^{A}6$/J	932	933	$^{S}7$
ν_{19} (A′)	737			741		
ν_{20} (A′)	533			533		
ν_{21} (A′)	511	522/518	$^{A}1$/C	509	515	B
ν_{22} (A′)	491	485	f	491	478/486	$^{AS}1$/e
ν_{23} (A′)	344			346	357	A
ν_{24} (A″)	954	959/963	$^{A}7$/g	970		
ν_{25} (A″)	877	866/858	$^{AS}2$/I	877	875	H
ν_{26} (A″)	824	832	$^{A}5$/h	824	832	$^{AS}3$
ν_{27} (A″)	753	761/763	$^{A}4$/G	771	763	F
ν_{28} (A″)	654	646/643	$^{A}3$/E	656	650/656	$^{S}3$/$^{S}8$
ν_{29} (A″)	563	579/581	$^{A}2$/D	582	572	$^{S}2$
ν_{30} (A″)	416	419	$^{AS}1$	418	422/418	$^{S}1$/d
ν_{31} (A″)	270			374	371/385	$^{S}6$/a
ν_{32} (A″)	209	203	c	211	215/203	$^{S}2$/$^{AS}4$
ν_{33} (A″)	183	175	b	183	184/190	a/$^{AS}2$

[a]The peaks, $^{A}1$–$^{A}14$, $^{S}1$–$^{S}7$, and $^{AS}1$–$^{AS}5$, refer to the labels used in Fig. 3 and Table II. The peaks labeled with letters refer to those used in the PE spectra (Figs. 2 and 4–6) and Table I.

the same, reflecting the slight different structures of the two conformers. In addition, more vibrational levels for the DBS of the *anti*-3HOP conformer are observed in the photodetachment spectrum, because of the broader excitation energy range as a result of the higher DBS binding energy of the *anti*-conformer, i.e., the lower excitation energy of the *anti*-conformer as defined by its 0–0 transition ($^{A}0'$ in Fig. 3).

C. Conformation-selective resonant PE spectra: Autodetachment involving DBS vibrational levels of single modes of *anti*- and *syn*-3HOP

Fig. 4 shows the resonant PE images and spectra of 3HOP that correspond to autodetachment from vibrational levels of single modes of the DBS for a given conformer. As shown previously,[28–32] autodetachment from vibrational levels of DBS generally follows the $\Delta v = -1$ propensity rule due to the similarity of the molecular structures in the DBS and the neutral,[24,25] that is, the *n*th vibrational level of a given mode

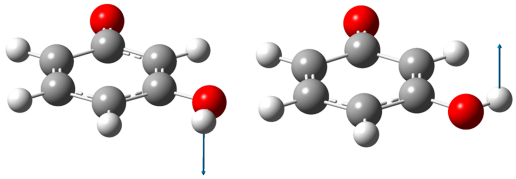

FIG. 7. The fundamental ν_{31} vibrational mode of *anti*- and *syn*-*m*-$HO(C_6H_4)O^{\cdot}$ and their calculated frequencies (Table III).

($\nu'_x{}^n$) of the DBS is favored to autodetach to the $(n-1)$th level of the corresponding neutral mode ($\nu_x{}^{n-1}$).[22] The vibrationally induced autodetachment involves a strong vibronic coupling, during which one vibrational quantum of mode ν'_x is transferred to the DBS electron. Hence, only modes with sufficiently high frequencies can couple with the DBS electron for the vibrationally induced autodetachment. In comparison to the relative intensities of peaks $^{S}0_0{}^{0}$ and $^{A}0_0{}^{0}$ in the non-resonant spectra in Fig. 2, the $^{A}0_0{}^{0}$ peak in Figs. 4(a)–4(c) and 4(e)–4(h) is highly enhanced while the $^{S}0_0{}^{0}$ peak is almost negligible, indicating autodetachment from fundamental vibrational levels ($^{A}\nu'_x{}^{1}$) of the DBS of the *anti*-*m*-$HO(C_6H_4)O^{-}$ conformer. The assignments of Figs. 4(a)–4(e) have been discussed in the recent preliminary study,[10] except one reassignment about the resonant peak ($^{A}1$) in Fig. 4(a), as mentioned above. The $^{A}1$ peak in the photodetachment spectrum (Fig. 3) was assigned to the $^{A}20'^{1}$ DBS level previously. However, on the basis of the PE spectra and the overtone excitation level in Fig. 4(j) (see below), the $^{A}1$ peak excited in Fig. 4(a) should be due to the $^{A}21'^{1}$ DBS level of the *anti*-3HOP conformer (Table II).

In Fig. 4(h), the detachment laser wavelength (515.83 nm) corresponds to the $^{A}7$ resonant peak in the photodetachment spectrum (Fig. 3). The shift of the $^{A}7$ peak relative to the $^{A}0'$ DBS ground vibrational level of the *anti*-conformer is measured to be 959 cm^{-1} (Table II), which is in good agreement with the computed frequency of the ν_{24} (A″) mode of *anti*-*m*-$HO(C_6H_4)O^{\cdot}$ (954 cm^{-1}, Table III). Thus, Fig. 4(h) corresponds to resonant excitation to the $^{A}24'^{1}$ DBS vibrational level of the *anti*-3HOP conformer, followed by autodetachment to the $^{A}0_0{}^{0}$ ground state of the neutral *anti*-*m*-$HO(C_6H_4)O^{\cdot}$ conformer according to the $\Delta v = -1$ propensity rule. Similarly, the PE spectra in Figs. 4(f) and 4(g) are due to autodetachment from the $^{A}26'^{1}$ and $^{A}18'^{1}$ DBS vibrational levels of the *anti*-3HOP conformer, respectively. The strong A peak in Fig. 4(f) is due to the near-threshold enhancement, similar to that observed in Fig. 2(a). The enhanced $^{S}0_0{}^{0}$ peak in Fig. 4(i) is due to autodetachment from the $^{S}28'^{1}$ DBS vibrational level of the *syn*-3HOP conformer. In Fig. 4(j), the $^{A}21^{1}$ vibrational level of the *anti*-*m*-$HO(C_6H_4)O^{\cdot}$ conformer (peak C) is greatly enhanced. According to the $\Delta v = -1$ propensity rule, the enhanced peak C should be from autodetachment of the $^{A}21'^{2}$ DBS vibrational level of the *anti*-3HOP conformer. Indeed, the photon energy used (513.61 nm) is shifted from the $^{A}0'$ DBS ground state of the *anti*-3HOP conformer by 1043 cm^{-1}, which is exactly twice the frequency measured for the $^{A}21'$ mode (Table II). Even though both the *anti*- and *syn*-3HOP conformers are present in the ion beam, the resonant excitation

to specific vibrational levels via the DBS allows conformer-specific and autodetachment-enhanced resonant PE spectra to be obtained.

D. Conformation-selective resonant PE spectra: Autodetachment from combinational DBS vibrational levels of *anti*- and *syn*-3HOP

Autodetachment from combinational vibrational levels of DBS is more complicated because of multiple autodetachment channels. For example, excitation to a two-mode, above-threshold combinational DBS vibrational level ($\nu_x'^m\nu_y'^n$) can autodetach to a final neutral level of either $\nu_x^{m-1}\nu_y^n$ or $\nu_x^m\nu_y^{n-1}$, following the $\Delta\nu = -1$ propensity rule and mode-selectivity. In Fig. 5(a), a single dominating peak **f** is observed at an electron binding energy of 19 402 cm^{-1} (Table I), which is not observed in the non-resonant PE spectrum in Fig. 2(b). Peak **f** has an energy shift of 485 cm^{-1} from the $^A0_0^0$ origin peak of the *anti*-conformer, which is in good agreement with the computed frequency of the ν_{22} (A′) mode of *anti-m*-HO(C_6H_4)O· (Table III). The photon energy used in Fig. 5(a) has a shift of 1004 cm^{-1} to $^A0'$, i.e., 485 cm^{-1} + 519 cm^{-1}, corresponding to a combinational DBS vibrational level $^A21'^122'^1$ of the *anti*-3HOP conformer. The 519 cm^{-1} vibrational frequency for the $^A\nu_{21}'$ mode deduced from the $^A8$ resonant peak agrees well with that from the $^A1$ resonant peak (522 cm^{-1} in Table II). The frequency for the $^A\nu_{21}'$ DBS mode is the same as that of the $^A\nu_{21}$ mode measured in the PE spectra for the neutral radical (518 cm^{-1} in Table I). In Fig. 5(a), only peak **f** ($^\mathbf{A}\mathbf{22^1}$) is enhanced because only one quantum of mode $^A\nu_{21}'$ (519 cm^{-1}) has enough energy to detach the DBS electron with a binding energy of 490 cm^{-1}. This is also the case in Fig. 5(b), where a combinational DBS vibrational level of $^A22'^129'^1$ is excited and only autodetachment to the final neutral level of $^\mathbf{A}\mathbf{22^1}$ is energetically possible.

Figs. 5(d), 5(g), and 5(i) display cases involving excitation to two-mode combinational DBS levels of the *anti*-3HOP conformer, in which each mode can couple to the DBS electron to induce autodetachment. Hence, two enhanced peaks are observed in each spectrum. However, in Figs. 5(h) and 5(j), only one peak (**I** $^\mathbf{A}\mathbf{25^1}$ in Fig. 5(h) and **g** $^\mathbf{A}\mathbf{24^1}$ in Fig. 5(j)) is enhanced, even though both modes of the excited DBS level ($^A21'^125'^1$ in Fig. 5(h) and $^A21'^124'^1$ in Fig. 5(j)) are energetically possible to induce autodetachment. This observation suggests that the coupling of the $^A\nu_{21}'$ mode with the DBS electron is much stronger than the $^A\nu_{24}'$ or $^A\nu_{25}'$ mode. Such mode-dependent vibronic coupling has been observed previously.[28–32] Figs. 5(c) and 5(e) show two more examples of mode-dependent vibrationally induced autodetachment. These two spectra involve resonant excitations to two-mode combinational DBS levels ($^S23'^130'^1$ and $^S22'^130'^1$, respectively) of the *syn*-3HOP conformer. In both cases, only one vibrational peak is observed to be enhanced (**A** $^\mathbf{S}\mathbf{23^1}$ in Fig. 5(c) and **e** $^\mathbf{S}\mathbf{22^1}$ in Fig. 5(e)), even though the frequencies of both DBS modes in each case are energetically possible to induce autodetachment. In these cases, the mode that couples with the DBS electron is the $^S\nu_{30}'$ mode.

Fig. 5(f) shows a case of the breakdown of the $\Delta\nu = -1$ propensity rule. The $^S6$ resonant peak (Fig. 3) corresponds to a three-mode combinational DBS vibrational level of the *syn*-3HOP conformer ($^S23'^131'^133'^1$ in Table II). However, only peak A ($^S23^1$) is enhanced in the resonant PE spectrum, suggesting the coupling of one quantum of ν_{31}' and one quantum of ν_{33}' simultaneously to the DBS electron during autodetachment. Such breakdown of the $\Delta\nu = -1$ propensity rule has been observed previously,[28–32] often involving low frequency DBS modes.

It is also worthwhile to point out that the resonantly enhanced peaks e, f, g in Fig. 5 due to autodetachment from combinational DBS vibrational levels represent new vibrational features that are not observed in the non-resonant PE spectra in Fig. 2, as shown in Table I. The weak peak c observed in Fig. 5(d) is also a new vibrational feature corresponding to the excitation of a low frequency bending mode ($^A\nu_{32}$) of the *anti-m*-HO(C_6H_4)O· conformer.

E. Autodetachment from overlapping DBS vibrational levels of *anti*- and *syn*-3HOP

For resonant excitations to overlapping DBS vibrational levels, the resonantly enhanced PE spectra can be even more complicated as a result of different autodetachment channels. Fig. 6 displays resonant PE spectra from overlapping DBS vibrational levels of three types: (1) those from the *anti*-3HOP conformer (Figs. 6(e) and 6(i)), (2) those from the *syn*-3HOP conformer (Figs. 6(c), 6(g), and 6(j)), and (3) those from both conformers (Figs. 6(a), 6(b), 6(d), 6(f), and 6(h)). The intensity ratio of the *anti*- and *syn*-conformers is defined by the $^S0_0^0$ and $^A0_0^0$ peaks in the non-resonant PE spectra shown in Fig. 2. Significant changes of the relative intensities of these two peaks in the resonant PE spectra indicate fundamental excitations of a specific DBS vibrational mode of a given conformer. In these cases, the fundamental vibrational frequency of a given DBS mode is degenerate with that of another mode or combinational modes. This happened in eight out of the ten spectra in Fig. 6. In Figs. 6(b), 6(e), and 6(i), the $^A0_0^0$ peak is enhanced relative to the $^S0_0^0$ peak, due to resonant excitations to the $^A25'^1$, $^A14'^1$, and $^A11'^1$ DBS levels of the *anti*-3HOP conformer, respectively. The frequencies for the three modes are given in Tables II and III. In Figs. 6(a), 6(c), 6(d), 6(g), and 6(h), the $^S0_0^0$ peak is enhanced relative to the $^A0_0^0$ peak, due to excitations to the $^S22'^1$, $^S29'^1$, $^S26'^1$, $^S18'^1$, and $^S17'^1$ of the *syn*-conformer, respectively, as shown in Tables II and III.

The overlapping combinational modes in Figs. 6(e) and 6(i) are also from the *anti*-conformer. In Fig. 6(e), both the **C** $^\mathbf{A}\mathbf{21^1}$ and **E** $^\mathbf{A}\mathbf{28^1}$ peaks are enhanced and the overlapping combinational mode can be straightforwardly assigned to the $^A21'^128'^1$ DBS level. In Fig. 6(i), the enhanced **C** $^\mathbf{A}\mathbf{21^1}$ and **h** $^\mathbf{A}\mathbf{26^1}$ peaks suggest excitation to the $^A21'^126'^1$ DBS level. Note that the **h** $^\mathbf{A}\mathbf{26^1}$ peak was not resolved from the dominating H peak in the non-resonant PE spectrum (Fig. 2(b) and Table I). It should also be pointed out that the H peak is significantly enhanced in Fig. 6(i). However, there are no DBS levels that can autodetach to this level of the neutral *syn*-conformer. We attribute the enhanced H peak to the threshold effects, which are observed for the A peak ($^S23^1$) in a number of detachment wavelengths (for example, in Figs. 2(a) and 4(f)).

The overlapping combination modes in Figs. 6(c) and 6(g) are all from the *syn*-conformer. In Fig. 6(c), a new peak **a** $^{S}\mathbf{33}^{1}$ is observed, suggesting excitation to the $^{S}31'^{1}33'^{1}$ combinational DBS level with only strong vibronic coupling by the $^{S}\nu_{31}'$ mode in the autodetachment. In Fig. 6(g), two peaks **B** $^{S}\mathbf{21}^{1}$ and **F** $^{S}\mathbf{27}^{1}$ are enhanced, suggesting two overlapping combinational DBS levels, $^{S}21'^{1}30'^{1}$ and $^{S}27'^{1}33'^{1}$, respectively, where again only one mode in each case is strongly coupled with the DBS electron for autodetachment. Fig. 6(j) also shows the same two enhanced peaks, **B** $^{S}\mathbf{21}^{1}$ and **F** $^{S}\mathbf{27}^{1}$, suggesting two overlapping combinational DBS levels, $^{S}21'^{1}28'^{1}$ and $^{S}27'^{1}30'^{1}$, respectively, also with only one mode in each case strongly coupled with the DBS electron.

The more complicated cases are those involving resonant excitations to overlapping DBS vibrational levels of both 3HOP conformers, as shown in Figs. 6(a), 6(b), 6(d), 6(f), and 6(h), corresponding to the resonant peaks $^{AS}1$–$^{AS}5$ in Fig. 3. In Fig. 6(a), in addition to the enhanced $^{S}0_{0}^{0}$ peak due to the excitation to the $^{S}22'^{1}$ DBS level of the *syn*-conformer, the **c** $^{A}\mathbf{32}^{1}$ peak is observed, suggesting an overlapping combinational DBS level of $^{A}30'^{1}32'^{1}33'^{1}$ in violation of the $\Delta v = -1$ propensity rule, because vibrational quanta ($^{A}30'^{1}33'^{1}$) are coupled to the DBS electron for the autodetachment to the $^{A}32^{1}$ final vibrational state. The strong peak A ($^{S}23^{1}$) is a result of threshold enhancement, as mentioned above. In Fig. 6(b), the enhanced peaks **b** $^{A}\mathbf{33}^{1}$ and **A** $^{S}\mathbf{23}^{1}$ imply excitation to an overlapping DBS level involving the two conformers, i.e., $^{A}21'^{1}33'^{2}/^{S}23'^{1}33'^{1}$. The enhanced **D** $^{A}\mathbf{29}^{1}$ peak in Fig. 6(d) suggests that the overlapping DBS level is $^{A}29'^{2}$. In Fig. 6(f), the enhanced **f** $^{A}\mathbf{22}^{1}$ and **B** $^{S}\mathbf{21}^{1}$ peaks suggest overlapping combinational DBS levels of $^{A}22'^{1}27'^{1}/^{S}21'^{1}32'^{2}$. Finally, in Fig. 6(h), the enhanced levels **d** $^{S}\mathbf{30}^{1}$ and **G** $^{A}\mathbf{27}^{1}$ imply two overlapping combinational DBS levels of $^{S}29'^{1}30'^{1}/^{A}27'^{1}29'^{1}$, in addition to the overlapping $^{S}17'^{1}$ DBS level. The strong H peak in Fig. 6(h) is attributed to threshold enhancement, similar to that in Fig. 6(i).

All the assignments for the observed DBS vibrational resonances in Fig. 3 are summarized in Table II. An energy level diagram is displayed in Fig. 8, showing the resonant excitations to the DBS vibrational levels of the two 3HOP conformers and the observed autodetachment channels. The electron detachment thresholds and the DBS binding energies for each conformer are also shown. Fig. 8 reveals the complexity of the 3HOP system due to the presence of the two conformers, as well as the wealth of spectroscopic information that can be obtained using resonant PES via the vibrational levels of the DBS. The experimental vibrational frequencies obtained for the two conformers of the *m*-HO(C_6H_4)O· radical are compared with the computed frequencies in Table III. In many cases, the same frequencies are measured from both the photodetachment spectrum of the DBS and the PE spectra (both resonant and non-resonant) for the neutral

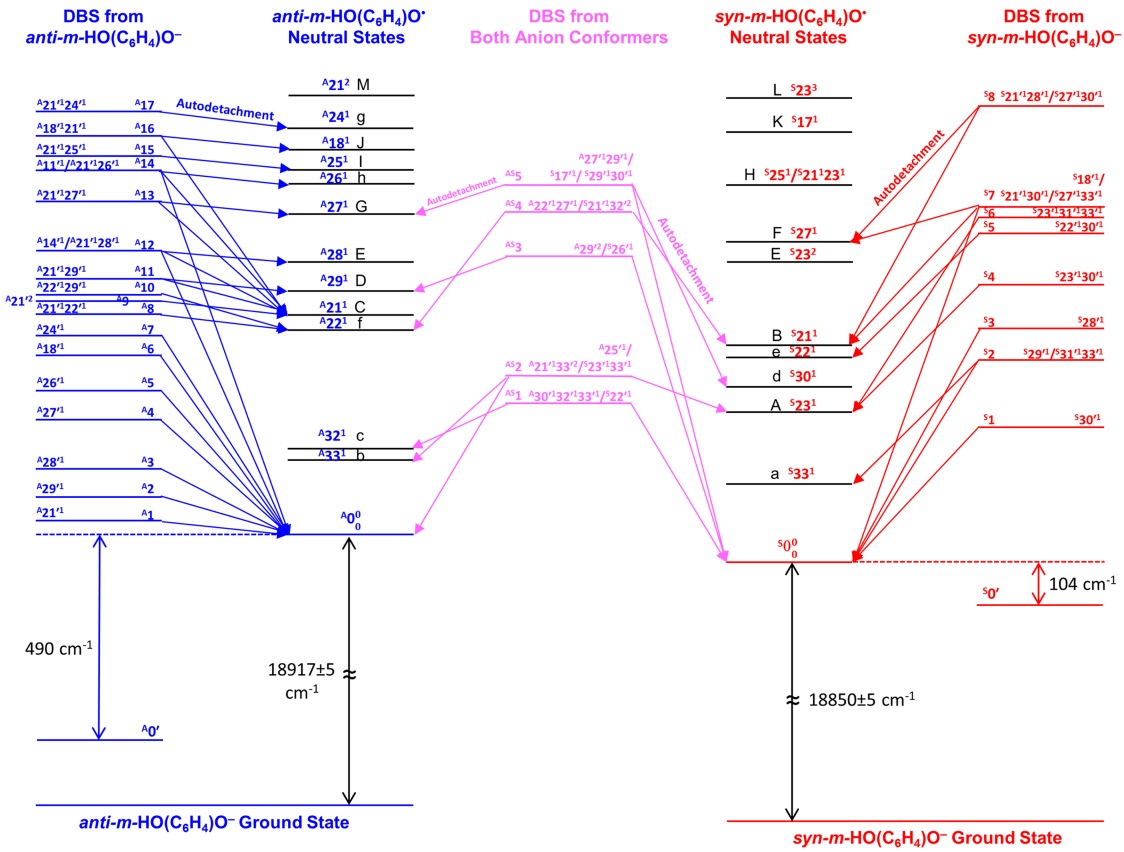

FIG. 8. A schematic energy level diagram for autodetachment from the DBS vibrational levels of the two conformers of 3HOP to the neutral final states of *anti*- and *syn*-*m*-HO(C_6H_4)O·. The detachment thresholds and the DBS binding energies of *anti*- and *syn*-*m*-HO(C_6H_4)O$^-$ are given. Autodetachment processes from DBS vibrational levels of different conformers are indicated by the arrows with different colors: blue for *anti*-*m*-HO(C_6H_4)O$^-$, red for *syn*-*m*-HO(C_6H_4)O$^-$, and pink for overlapping DBS levels of the two conformers. The DBS peak labels and the peak labels from the PE spectra are given. The assignments of the final neutral states and the DBS levels are given in Tables I and II, respectively.

radicals. They are generally in agreement within the experimental uncertainties.

F. Comments about the conformation selectivity

As shown in Fig. 1, the different orientation of the hydrogen atom on the hydroxyl group results in the two conformers of 3HOP. The intensity ratio of the 0–0 detachment transitions ($^{S}0_0^0$ vs. $^{A}0_0^0$) in Fig. 2 suggests that the *syn*-conformer is more stable, consistent with a previous B3LYP calculation, which suggested that *anti*-3HOP is 0.855 kcal/mol higher in energy.[5] Upon electron detachment, the corresponding neutral radicals, *anti*- and *syn*-*m*-$HO(C_6H_4)O^{\cdot}$, are obtained and their electron affinities are different by 67 cm^{-1} with the *anti*-conformer being slightly higher. Table III reveals that the vibrational frequencies of the neutral radicals of the two conformers are very similar, except mode ν_{31}. As shown in Fig. 7, this mode is the out-of-plane rocking mode of the –OH group and is related to the conversion of the two conformations. It is interesting to note that the frequency of this mode in the *syn*-conformer is much higher. At room temperature, these modes would be significantly populated, leading to equilibrium or free conversion of the two conformers. At lower temperatures, the two conformers are frozen out, but would not be separable. However, using resonant excitations to certain vibrational levels of the DBS, pure or nearly pure conformers of the neutral radicals can be produced. It was shown previously that resonant excitation to an intermediate electronic state of an anion allows different final neutral states to be accessed.[40] Fundamental excitations to single DBS vibrational modes of a given conformer can produce almost pure conformers of the corresponding neutral radical in its vibrational ground state according to the $\Delta\nu = -1$ autodetachment propensity rule. For example, using photodetachment wavelengths corresponding to those used in Figs. 4(a)–4(c), 4(e), and 4(g), one can produce almost pure neutral *anti*-*m*-$HO(C_6H_4)O^{\cdot}$ radicals, whereas using the wavelength corresponding to that used for Fig. 4(d), one can produce almost pure neutral *syn*-*m*-$HO(C_6H_4)O^{\cdot}$ radicals. A neutral conformer with specific vibrational energy can also be produced such as that in Fig. 4(j) or Fig. 5(a). Hence, resonant photodetachment may be a good technique to produce conformer-selected beams of neutral dipolar species for further investigations of conformation-dependent chemical and physical properties.

V. CONCLUSIONS

In conclusion, we report an extensive investigation of the photodetachment spectroscopy of cryogenically cooled *m*-$HO(C_6H_4)O^{-}$ anions and resonant photoelectron imaging via vibrational levels of the dipole-bound excited states. Two conformers are observed for this anion and each possesses an excited dipole-bound state just below the detachment threshold. Thirty DBS vibrational resonances are observed for the two conformers with some of the resonances consisting of overlapping vibrational levels. Thirty resonant photoelectron spectra are obtained by tuning the detachment laser to each of the vibrational resonances. Extensive spectroscopic information is obtained for each of the conformers. The vibrational structures are assigned using computed frequencies of the two conformers and by using the resonant PE spectra on the basis of the propensity rule of vibrationally induced autodetachment from DBS. Resonant photoelectron spectroscopy of cold anions is shown to be an effective method to probe the spectroscopy of conformers of dipolar molecular species with sufficient dipole moments to support dipole-bound states.

ACKNOWLEDGMENTS

We would like to thank Dr. Hong-Tao Liu and Dr. Chuan-Gang Ning for experimental assistance and valuable discussions. This work was supported by the National Science Foundation.

[1] P. Seta, E. Bienvenue, A. L. Moore, P. Mathis, R. V. Bensasson, P. Liddell, P. J. Pessiki, A. Joy, T. A. Moore, and D. Gust, Nature **316**, 653 (1985).
[2] M. S. Graige, M. L. Paddock, J. M. Bruce, G. Feher, and M. Y. Okamura, J. Am. Chem. Soc. **118**, 9005 (1996).
[3] M. H. V. Huynh and T. J. Meyer, Chem. Rev. **107**, 5004 (2007).
[4] M. Altarawneh, B. Z. Dlugogorski, E. M. Kennedy, and J. C. Mackie, J. Phys. Chem. A **114**, 1098 (2010).
[5] X. B. Wang, Q. Fu, and J. Yang, J. Phys. Chem. A **114**, 9083 (2010).
[6] C. Desfrancois, H. Abdoul-Carmine, and J. P. Schermann, "Ground-state dipole-bound anions," Int. J. Mod. Phys. B **10**, 1339 (1996).
[7] N. I. Hammer, R. J. Hinde, R. N. Compton, K. Diri, K. D. Jordan, D. Radisic, S. T. Stokes, and K. H. Bowen, J. Chem. Phys. **120**, 685 (2004).
[8] R. L. Jackson, P. C. Hiberty, and J. I. Brauman, J. Chem. Phys. **74**, 3705 (1981).
[9] K. Yokoyama, G. W. Leach, J. B. Kim, W. C. Lineberger, A. I. Boldyrev, and M. Gutowski, J. Chem. Phys. **105**, 10706 (1996).
[10] D. L. Huang, H. T. Liu, C. G. Ning, and L. S. Wang, J. Phys. Chem. Lett. **6**, 2153 (2015).
[11] J. I. Seeman, Chem. Rev. **83**, 83 (1983).
[12] A. Gutteridge and J. Thornton, FEBS Lett. **567**, 67 (2004).
[13] J. P. Simons, R. A. Jockusch, P. CarCabal, I. Hunig, R. T. Kroemer, N. A. Macleod, and L. C. Snoek, Int. Rev. Phys. Chem. **24**, 489 (2005).
[14] A. Mardyukov, H. Quanz, and P. R. Schreiner, Nat. Chem. **9**, 71 (2017).
[15] B. C. Dian, G. G. Brown, K. O. Douglass, and B. H. Pate, Science **320**, 924 (2008).
[16] B. C. Dian, J. R. Clarkson, and T. S. Zwier, Science **303**, 1169 (2004).
[17] S. T. Park, S. K. Kim, and M. S. Kim, Nature **415**, 306 (2002).
[18] M. H. Kim, L. Shen, H. Tao, T. J. Martinez, and A. G. Suits, Science **315**, 1561 (2007).
[19] T. R. Rizzo, J. A. Stearns, and O. V. Boyarkin, Int. Rev. Phys. Chem. **28**, 481 (2009).
[20] F. Filsinger, U. Erlekam, G. von Helden, J. Kupper, and G. Meijer, Phys. Rev. Lett. **100**, 133003 (2008).
[21] Y. P. Chang, K. Dlugolecki, J. Kupper, D. Rosch, D. Wild, and S. Willitsch, Science **342**, 98 (2003).
[22] H. T. Liu, C. G. Ning, D. L. Huang, P. D. Dau, and L. S. Wang, Angew. Chem., Int. Ed. **52**, 8976 (2013).
[23] L. S. Wang, J. Chem. Phys. **143**, 040901 (2015).
[24] R. S. Berry, J. Chem. Phys. **45**, 1228 (1966).
[25] J. Simons, J. Am. Chem. Soc. **103**, 3971 (1981).
[26] I. Leon, Z. Yang, and L. S. Wang, J. Chem. Phys. **139**, 194306 (2013).
[27] I. Leon, Z. Yang, and L. S. Wang, J. Chem. Phys. **138**, 184304 (2013).
[28] D. L. Huang, H. T. Liu, C. G. Ning, and L. S. Wang, J. Chem. Phys. **142**, 124309 (2015).
[29] D. L. Huang, H. T. Liu, C. G. Ning, G. Z. Zhu, and L. S. Wang, Chem. Sci. **6**, 3129 (2015).
[30] D. L. Huang, G. Z. Zhu, and L. S. Wang, J. Chem. Phys. **142**, 091103 (2015).
[31] D. L. Huang, H. T. Liu, C. G. Ning, P. D. Dau, and L. S. Wang, Chem. Phys. **482**, 374 (2017).
[32] D. L. Huang, G. Z. Zhu, Y. Liu, and L. S. Wang, J. Mol. Spectrosc. **332**, 86 (2017).
[33] X. B. Wang and L. S. Wang, Rev. Sci. Instrum. **79**, 073108 (2008).
[34] I. León, Z. Yang, H. T. Liu, and L. S. Wang, Rev. Sci. Instrum. **85**, 083196 (2014).

[35]G. A. Garcia, L. Nahon, and I. Powis, Rev. Sci. Instrum. **75**, 4989 (2004).
[36]V. Dribinski, A. Ossadtchi, V. A. Mandelshtam, and H. Reisler, Rev. Sci. Instrum. **73**, 2634 (2002).
[37]H. T. Liu, C. G. Ning, D. L. Huang, and L. S. Wang, Angew. Chem., Int. Ed. **53**, 2464 (2014).
[38]D. L. Huang, P. D. Dau, H. T. Liu, and L. S. Wang, J. Chem. Phys. **140**, 224315 (2014).
[39]G. Z. Zhu and L. S. Wang, J. Chem. Phys. **143**, 221102 (2015).
[40]H. T. Liu, D. L. Huang, Y. Liu, L. F. Cheung, P. D. Dau, C. G. Ning, and L. S. Wang, J. Phys. Chem. Lett. **6**, 637 (2015).